

SHI, H., WANG, S., FERNANDEZ, C., YU, C., LI, X. and ZOU, C. 2020. Adaptive iterative working state prediction based on the double unscented transformation and dynamic functioning for unmanned aerial vehicle lithium-ion batteries. *Measurement and control* [online], 53(9-10), pages 1760-1773. Available from: <https://doi.org/10.1177/0020294020923057>

# Adaptive iterative working state prediction based on the double unscented transformation and dynamic functioning for unmanned aerial vehicle lithium-ion batteries.

SHI, H., WANG, S., FERNANDEZ, C., YU, C., LI, X. and ZOU, C.

2020

*This article is distributed under the terms of the Creative Commons Attribution 4.0 License (<https://creativecommons.org/licenses/by/4.0/> which permits any use, reproduction and distribution of the work without further permission provided the original work is attributed as specified on the SAGE and Open Access pages (<https://us.sagepub.com/en-us/nam/open-access-at-sage>).*

# Adaptive iterative working state prediction based on the double unscented transformation and dynamic functioning for unmanned aerial vehicle lithium-ion batteries

Measurement and Control  
2020, Vol. 53(9-10) 1760–1773  
© The Author(s) 2020  
Article reuse guidelines:  
sagepub.com/journals-permissions  
DOI: 10.1177/0020294020923057  
journals.sagepub.com/home/mac  


Haotian Shi<sup>1</sup>, Shunli Wang<sup>1</sup> , Carlos Fernandez<sup>2</sup>, Chunmei Yu<sup>1</sup>, Xiaoxia Li<sup>1</sup> and Chuanyun Zou<sup>1</sup>

## Abstract

In lithium-ion batteries, the accuracy of estimation of the state of charge is a core parameter which will determine the power control accuracy and management reliability of the energy storage systems. When using unscented Kalman filtering to estimate the charge of lithium-ion batteries, if the pulse current change rate is too high, the tracking effects of algorithms will not be optimal, with high estimation errors. In this study, the unscented Kalman filtering algorithm is improved to solve the above problems and boost the Kalman gain with dynamic function modules, so as to improve system stability. The closed-circuit voltage of the system is predicted with two non-linear transformations, so as to improve the accuracy of the system. Meanwhile, an adaptive algorithm is developed to predict and correct the system noises and observation noises, thus enhancing the robustness of the system. Experiments show that the maximum estimation error of the second-order Circuit Model is controlled to less than 0.20V. Under various simulation conditions and interference factors, the estimation error of the unscented Kalman filtering is as high as 2%, but that of the improved Kalman filtering algorithm are kept well under 1.00%, with the errors reduced by 0.80%, therefore laying a sound foundation for the follow-up research on the battery management system.

## Keywords

Lithium-ion batteries, working state, double unscented transformation, unscented Kalman filter, adaptive noise correction

Date received: 3 January 2020; accepted: 7 April 2020

## Introduction

With the widespread using of lithium-ion battery (LiB) in industry, daily life and the rise of dynamic wireless power transmission technology,<sup>1</sup> the estimation of state of charge (SOC) has become an important part of battery management. However, due to the complex structure of the battery, the SOC estimation is difficult because the SOC state of the battery is affected by the discharge current, internal temperature of the battery, self-discharge, aging and other factors. SOC of LiB is also the key of unmanned aerial vehicle (UAV) battery management system (BMS). Accurate estimation of the nuclear power status of LiBs can not only make the utilization of batteries more efficient but also facilitate the rational and effective management of LiBs, so as to improve the performance and safety of UAV. Due to the influence of various internal and external factors in the use of UAV power LiB, it is unable to accurately

estimate SOC. Nowadays, with the continuous development of new energy and deep studies of LiB, a few new kinds of accurate estimation methods are successively put forward for SOC ampere-hour integral measurements with simple operations. The early SOC estimation methods have very strong dependence. If the initial SOC is inaccurate, the estimated error will be accumulated gradually, finally deviating from the real and estimated values.<sup>2</sup> The open-circuit voltage (OCV) method

<sup>1</sup>School of Information Engineering, Engineering and Technology Center, Southwest University of Science and Technology, Mianyang, China

<sup>2</sup>School of Pharmacy & Life Sciences, Robert Gordon University, Aberdeen, UK

### Corresponding author:

Shunli Wang, School of Information Engineering, Engineering and Technology Center, Southwest University of Science and Technology, Mianyang 621010, China.

Email: wangshunli@swust.edu.cn



Creative Commons CC BY: This article is distributed under the terms of the Creative Commons Attribution 4.0 License (<https://creativecommons.org/licenses/by/4.0/>) which permits any use, reproduction and distribution of the work without

further permission provided the original work is attributed as specified on the SAGE and Open Access pages (<https://us.sagepub.com/en-us/nam/open-access-at-sage>).

uses battery OCV and nonlinear relation between the SOC and the lithium battery SOC estimate, but the battery Small OCV measurement deviation errors may also occur in SOC. And measuring the OCV needs the battery to stand for a long time, so the OCV method cannot accurately estimate the SOC of the batteries in working states. The OCV method is not accurate to estimate the SOC of the battery's working state.<sup>3</sup>

The extended Kalman filter (EKF) algorithm is one of the most commonly used<sup>4</sup> SOC estimation algorithms, and the EKF algorithm is used to evaluate the power and energy of the hybrid system of LiB and ultra-capacitors, which solves the estimation error caused by system interference and sensor noise,<sup>5</sup> but EKF needs to calculate the Jacobi matrix of each cycle, which leads to a large amount of calculation. Adaptive EKF is used to estimate the working state of LiBs, which solves the limitation of EKF in SOC estimation of LiBs.<sup>6</sup> The fractional-order model is applied to the short circuit fault diagnosis of electric vehicle (EV) batteries,<sup>7</sup> and the fractional-order model is used to estimate the state of the hybrid power system of LiBs and ultra-capacitors, which fills the gap in the research on the remaining power estimation of hybrid power systems.<sup>8</sup> In addition, an enhanced equivalent circuit model (ECM) considering charge redistribution, health state and temperature effect is proposed.<sup>9</sup> The ECM of pure EV LiBs is analyzed.<sup>10</sup> A dynamic linear model-based charging state estimation method for LiBs is studied,<sup>11</sup> which is also EKF state analysis of LiBs in EV charge estimation.<sup>12</sup> A joint estimation method of SOC and state of energy (SOE) based on the particle filtering is proposed, which greatly reduces the problem of cumulative error due to current or voltage measurement noise.<sup>13</sup> A method for estimating the SOC of a LiB considering capacity attenuation is proposed.<sup>14</sup> The OCV and charging state function of no-load LiBs are optimized.<sup>15</sup> The parameter identification method of the ECM of aviation LiBs is studied<sup>16</sup> and the health status is evaluated and analyzed.<sup>17</sup>

Aiming at the problem that large initial SOC error leads to the accumulation of subsequent SOC estimation error, a fractional-order model-based estimation method for SOC of LiBs is proposed.<sup>18</sup> In addition, a new method for predicting the life of LiBs based on the voltage change rate and iterative calculation is proposed.<sup>19</sup> The online dynamic equilibrium adjustment of high-power LiB packs based on the equilibrium state estimation is designed.<sup>20</sup> The method of data model fusion is applied to the estimation of online charging state and health state of LiB.<sup>21</sup> The particle filter (PF) method was used to estimate LiFePO<sub>4</sub> batteries, which solved the interference problem caused by temperature changes and drift current noise in SOC estimation.<sup>22</sup> The charge state and deformation rate of the electrochemical cell are studied.<sup>23</sup> The dual-scale adaptive PF algorithm is also applied to online parameter state estimation of LiBs, which solves the problem of large workload and inaccurate state estimation in offline

state.<sup>24</sup> With the continuous deepening of research, the battery's hysteresis effect is considered in the ECM, and the unscented PF is used to predict the discharge state and the remaining discharge time, which improves the accuracy and convergence speed of SOC estimation under dynamic driving cycles.<sup>25</sup> The support vector machine (SVM) is also applied in the accurate estimation of SOC of LiBs,<sup>26</sup> and a vehicle battery predictive charge control model based on the vehicle state prediction is established,<sup>27</sup> and their estimation accuracy is similar to EKF. In addition to this, to solve the problem of accurate estimation of aviation LiB pack, a safety prediction and estimation method based on the real-time detection and filtering is proposed.<sup>28</sup> To avoid a lot of work of offline estimation, the battery model and online estimation of LiB charging state are studied.<sup>29</sup> Using the principle of artificial intelligence to solve, the neural network gives the optimal decision, optimizes its energy consumption method in the corresponding building area and improves the utilization efficiency of LiBs.<sup>30</sup> A power state estimation model based on the classification regression tree is studied and used in hybrid cars.<sup>31</sup> A new power management method is proposed and applied to V2V, V2B/I, V2N and other connected vehicles, which greatly reduces energy consumption.<sup>32</sup> The charging state model of LiBs is established to facilitate the high efficiency of industrial application.<sup>33</sup> A model-based untraceable Kalman filter observer is designed and used in charge state estimation of LiBs.<sup>34</sup> An online model identification and state-of-charge estimation method for LiBs based on the recursive least squares observer is proposed,<sup>35</sup> and a hybrid energy storage system based on the energy distribution strategy for four-wheel-drive EVs is studied.<sup>36</sup>

In addition to the above, many SOC estimation algorithms have added the latest technologies. By using the untracked Kalman filter (UKF) algorithm, an accurate equivalent circuit modeling method of LiB based on the recurrent neural network is proposed.<sup>37</sup> The synergy method of EKF and UKF is used to estimate the SOC of LiB, which improves the robustness and stability of the BMS system.<sup>38</sup> The modified neural network model is combined with EKF to estimate the SOC of LiB.<sup>39</sup> An onboard adaptive model for LiB state estimation based on the proportional integral error adjustment Kalman filter is established and studied.<sup>40</sup> In addition, an accurate charge state estimation of LiB based on the model mismatch is proposed.<sup>41</sup> By constructing observer, an enhanced SOC estimation model and its online parameter identification are established,<sup>42</sup> and a method for LiB model identification and charging state estimation based on the iterative learning is proposed.<sup>43</sup> An LiB model based on the new reduced-order electrochemistry was established and the estimation method of the SOC is given.<sup>44</sup> The health diagnosis method of LiB energy storage based on the mechanism recognition model is studied.<sup>45</sup>

An improved UKF algorithm is used for SOC estimation of LiBs, and two nonlinear transformations are

**Table 1.** Advantages and disadvantages of different models.

Models	The advantages and disadvantages
<i>Rint</i>	The circuit parameters are simple, but the dynamic characteristics of the battery cannot be reflected.
RC	It makes up for the deficiency of the <i>Rint</i> model, but the circuit equation is very complicated and the establishment of the model state equation is relatively difficult.
Thevenin	It has the advantages of <i>Rint</i> model and Resistance-Capacitance (RC) model, but the model regards the internal resistance of the battery as a constant value, which cannot represent the steady-state change of the battery voltage, and is not easy to estimate the running time of the battery.
PNGV	It makes up for the shortcoming of the Thevenin model, which is relatively simple and easy to identify parameters in the model.
GNL	Two parallel RC circuits are applied to characterize the transient and transient changes of battery voltage, respectively, and the self-discharge module is added. However, it is difficult to identify the model parameters.

PNGV: partnership for a new generation of vehicles; GNL: general nonlinear; RC, Resistance-Capacitance.

used to improve the accuracy of the system, under the premise of ensuring the stability of the system. The Kalman gain is improved and adaptive dynamic gain adjustment module is added to solve the problem of SOC value oscillation when the state of BMS changes suddenly. To solve the influence of noise on system stability, an adaptive algorithm is proposed to predict and correct system noise and observation noise, which can effectively reduce noise error and enhance system stability.

## Mathematical analysis

### ECM

The LiB models mainly include pure mathematical model, electrochemical mechanism model, thermal management model and ECM, among which the ECM is the most widely used. Common ECMs include *Rint*, Resistance -Capacitance (RC), Thevenin, partnership for a new generation of vehicles (PNGV) and general nonlinear (GNL) models. The advantages and disadvantages of the above common ECMs are shown in Table 1.

Because the working condition of UAV is more complicated, it requires higher precision of the model. Among the above five models, PNGV and GNL models have the highest accuracy. Compared with the GNL model, PNGV model has simple structure and less difficulty in model identification, which meets the requirements of parameter measurement in dry environment under complex working conditions of UAV. However, as the PNGV model could not completely represent the relaxation effect of the battery, this paper improved it and simulated the unrepresented relaxation effect in the original PNGV model through another parallel RC branch, so as to make it more fully meet the requirements of parameter measurement under the complicated working conditions of UAV. Therefore, the second-order circuit model (S-OCM) is more suitable for characterizing battery status in dynamic environments. The circuit coupling relationship of the S-OCM is shown in Figure 1.

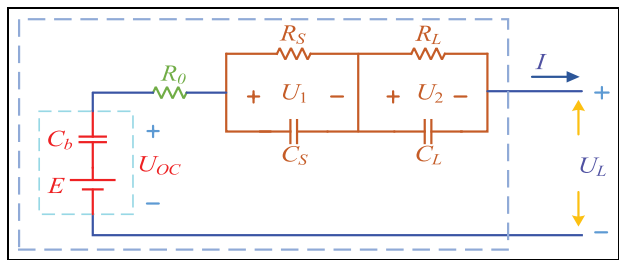


**Figure 1.** The second-order circuit model.

In the above S-OCM, on the basis of the PNGV model, a parallel RC circuit was added and  $E$  is the ideal voltage source.  $R_0$  is the ohm resistance.  $R_S$  and  $R_L$  are the polarization resistance.  $C_S$  and  $C_L$  are the polarization capacitance. Among them, the parallel circuit composed of  $R_S$  and  $C_S$  has a small time constant, which is used to simulate the process of rapid voltage change when the current changes suddenly. The parallel circuit composed of  $R_L$  and  $C_L$  is used to simulate the rapid change of voltage when the current changes suddenly because their time constant is relatively large. The battery charging and discharging current takes  $I$  as the parameter and  $U_L$  as the battery terminal voltage. The S-OCM can better characterize the polarization characteristics of the battery, and it lays a foundation for UAV to maintain high stability and robustness when flying in the ever-changing environment.

The calculation of ampere-hour integration is as follows

$$SOC(t) = SOC(t_0) - \int_{t_0}^t \frac{\eta_T \eta_I I}{Q_N} d\tau \quad (1)$$

wherein  $SOC(t_0)$  and  $SOC(t)$  represent the SOC value of the battery at the initial time and at time  $t$ , respectively.  $I$  is the charge and discharge current, and  $\eta_I$  represents the coulomb efficiency at different  $I$ .  $T$  is the ambient temperature, and  $\eta_T$  represents the influence coefficient of different  $T$  on  $\eta_I$ .  $Q_N$  is the rated capacity. According to the S-OCM, selecting SOC as the unique

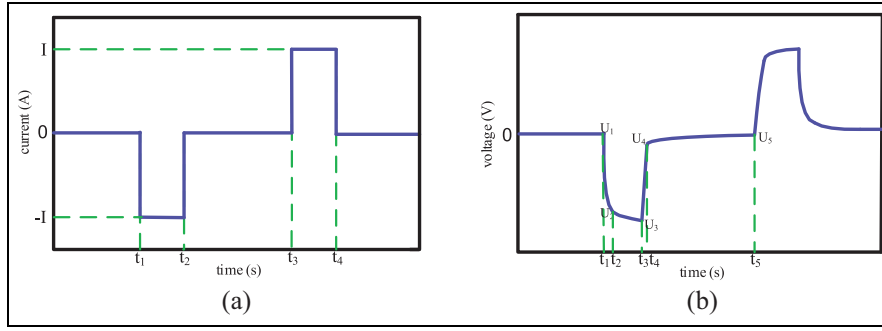


**Figure 2.** Schematic diagram of current and voltage curves in HPPC experiment: (a) the HPPC single-cycle current profile and (b) the HPPC single-cycle voltage profile.

**Table 2.** HPPC test steps of the main discharge process.

Step 1	The LiB is discharged in the standard discharge. After that, let the battery rest for 2 h and then charge the battery to 100% SOC with constant current and voltage. Where the charging current is set as 1 C (68 A h), the charging voltage is set as 4.2 V, and the cutoff condition is set as 3.4 A.
Step 2	Let the battery rest for 12 h to activate the battery and measure and record the voltage values at both ends of the battery.
Step 3	The current pulse test is carried out on the LiB. First discharge at 1-C current for 10 s, then maintain for 40 s and then charge at 1-C current for 10 s. The purpose is to make the battery return to the SOC value before discharge and complete a set of pulse charging and discharging tests.
Step 4	Start discharging with 0.5-C current, discharge for 12 min (remaining 90% SOC of the battery) and then let it rest for 1 h. The cutoff condition is 3 V.
Step 5	Repeat steps (3) and (4); each cycle discharges 10% capacity, record the SOC 0.9, 0.8, 0.7, ..., 0.1 at the relevant data and prepare for the next parameter identification.

HPPC: hybrid pulse power characterization; SOC: state of charge.

state variable of the system in the algorithm greatly reduces the computational complexity and enhances the timeliness of the algorithm. According to the positive direction selected above, the discrete form of the LiB state space equation is described as follows

$$\begin{cases} SOC(k) = SOC(k-1) - \frac{\eta_r \eta_l T_s}{Q_N} I(k-1) + w_{k-1} \\ U_L(k) = U_{oc}(SOC(k)) - R_s \left(1 - e^{-\frac{T_s}{C_s R_s}}\right) I(k-1) - R_L \left(1 - e^{-\frac{T_s}{C_L R_L}}\right) I(k-1) - R_0 I(k-1) + v_k \end{cases} \quad (2)$$

wherein  $T_s$  is the sampling time and  $w_{k-1}$  and  $v_k$  are the system noises, which are not related to each other.

**Parameter identification**

In view of the difference in the internal resistance of LiBs in the charging and discharging process, the selected LiBs are tested with the hybrid pulse power

**Table 3.** The features of voltage response curve of HPPC test.

Features (1)	The voltage at time $t_1$ and time $t_2$ is vertically changed, which is caused by the ohm resistance of the battery.
Features (2)	During $t_1 \sim t_2$ , the discharge current charges the polarization capacitor, which is the zero-state response of the double RC series circuit.
Features (3)	During $t_2 \sim t_3$ , discharge of polarization capacitor to polarization resistance, it is a zero-input response of a double RC series circuit.
Features (4)	Due to the existence of the energy storage capacitor, the terminal voltage $U_1$ is slightly higher than the terminal voltage $U_5$ .

HPPC: hybrid pulse power characterization; RC, Resistance - Capacitance.

characterization (HPPC) test of the main charging process and HPPC test of the main discharging process. The HPPC test steps of the main discharge process are summarized in Table 2.

Similarly, change the above fourth step to start charging at 0.5-C current. The charging time is 12 min, and the experimental data are recorded, which is the HPPC test process of the main charging process. The change of voltage and current of a single group in the HPPC experiment is shown in Figure 2.

The features of the voltage response curve of the HPPC test are used for parameter identification, and the features are shown in Table 3.

It can be seen from Table 2 that the values of  $R_0$  and  $C_b$  in the S-OCM can be directly obtained from features (1) and (4). The parameter values of the double RC circuit can be identified according to the battery terminal curve of features (2) and (3).

According to feature (1), the sudden change in the terminal voltage of the battery at the start and stop of discharge is caused by the ohm internal resistance.

Therefore, the ohm internal resistance can be calculated through the ohm law, as shown in equation (3)

$$R_0 = \frac{(U_1 - U_2) + (U_4 - U_3)}{2I} \quad (3)$$

When the LiB is in the pulse discharge stage of HPPPC experiment, let the flow direction of  $I_b$  be the positive direction of current. According to the reference direction of voltage and current in the figure, Kirchhoff's current law (KCL) and Kirchhoff's voltage law (KVL) equations can be listed, as shown in equation (4)

$$\begin{cases} dU_1/dt = i(t)/C_S - U_1/R_S C_S \\ dU_2/dt = i(t)/C_L - U_2/R_L C_L \\ U_L = U_{OC}(SOC) - i(t)R_0 - U_1 - U_2 \end{cases} \quad (4)$$

wherein  $U_1$  is the terminal voltage of the parallel circuit composed of  $R_S$  and  $C_S$  and  $U_2$  is a shunt terminal composed of  $R_L$  and  $C_L$ .

According to Figure 2(a), the battery is constantly exiled for 10s during  $t_1 \sim t_3$  and remained in a static state for the rest of the time. By time-domain analysis of two RC circuits in series, the voltage of RC network can be obtained as shown in equation (5)

$$U_1 = \begin{cases} R_S i(t) \left[ 1 - e^{-\frac{(t-t_1)}{\tau_S}} \right] & t_1 < t < t_2 \\ U_S(t_2) e^{-\frac{(t-t_2)}{\tau_S}} & t_2 < t < t_3 \end{cases} \quad (5)$$

$$U_2 = \begin{cases} R_L i(t) \left[ 1 - e^{-\frac{(t-t_1)}{\tau_L}} \right] & t_1 < t < t_2 \\ U_L(t_2) e^{-\frac{(t-t_2)}{\tau_L}} & t_2 < t < t_3 \end{cases}$$

wherein  $t_1$  is the start time of discharge,  $t_2$  is the stop time of discharge and  $t_3$  is the shelving stop time.  $\tau_S$  is the time constant of  $R_S$  and  $C_S$  parallel circuits,  $\tau_L$  is the time constant of  $R_L$  and  $C_L$  parallel circuits. The calculation formulas of  $\tau_S$  and  $\tau_L$  are shown in equation (6)

$$\tau_S = R_S C_S, \quad \tau_L = R_L C_L \quad (6)$$

Related to the SOC of the battery are: the battery during discharge, polarization capacitance  $C_S$  and  $C_L$  in charging status, the voltage of the parallel connection circuit of  $R_C$  exponential rise, after the batteries from discharge into the quiet place, capacitance  $C_S$  and  $C_L$  to separate parallel resistance discharge, and the voltage value of  $R_C$  parallel circuit drops. When using Matlab for HPPPC experimental data curve fitting, the reuse method of undetermined parameters can be calculated for values of the  $R_S$ ,  $R_L$ ,  $C_S$  and  $C_L$  in the S-OCM. The specific methods are shown in Table 4.

### Iterative calculation

The interior of the LiB is a typical nonlinear system. The battery OCV, battery internal resistance, battery terminal voltage and battery charge state all show

**Table 4.** The experimental procedure of HPPPC test.

Step 1	First, the experimental data from $U_4$ to $U_5$ in Figure 2(b) are taken out to prepare for data fitting.
Step 2	Write the output equation of the battery terminal voltage by the features (3), as shown in equation (7). $U_L = U_{OC} - IR_S e^{-\frac{t}{\tau_S}} - IR_L e^{-\frac{t}{\tau_L}}$ (7)
Step 3	Simplify parameter identification, as shown in equation (8). $U_L = f - ae^{-ct} - be^{-dt}$ (8)
Step 4	Take $f$ , $a$ , $b$ , $c$ and $d$ as the undetermined parameters, take equation (8) as the objective equation to carry out double exponential curve fitting.
Step 5	According to the fitting results of the double exponential curve, by comparing equations (7) and (8), the result of parameter identification is shown in equation (9).

$$\begin{cases} U_{OC} = f \\ R_S = a/I \\ R_L = b/I \\ C_S = 1/(R_S c) \\ C_L = 1/(R_L d) \end{cases} \quad (9)$$

HPPPC: hybrid pulse power characterization.

strong nonlinear changes under battery operating conditions. The nonlinear Kalman filter includes EKF, UKF and so on. The forced transformation of EKF's nonlinear system into a linear system will cause the Taylor truncation error. The method of neglecting higher order terms may diverge filtering and cause the algorithm to fail. When the nonlinear strength of the system is high, the effect of EKF is not ideal. UKF is based on the unscented transformations and uses a suitable sampling strategy to approximate the distribution of state variables; the error introduced in EKF algorithm due to ignoring higher order terms is avoided. At the same time, there is no need to repeatedly calculate the complex Jacobian matrix, which makes the calculation difficult. However, according to the estimation effect under simulated dynamic conditions, when the pulse current change rate is large, the estimation error of the UKF algorithm is large. To solve the problem, the UKF algorithm is improved on the premise of the same estimation accuracy and adaptive algorithm is added into the improved UKF to predict and modify the system noise and observed noise, effectively reducing the estimation error.

**Nonlinear transformation.** Nonlinear transformation is the core of UKF algorithm, and its basic principle is to characterize the probability density distribution of random variables with appropriate distribution of

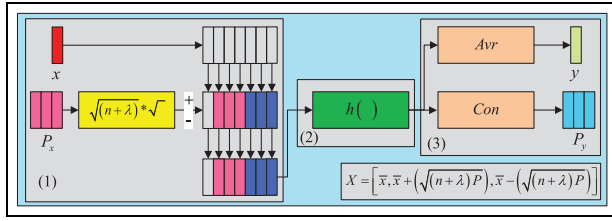


**Figure 3.** Unscented transformation schematic.

sampling points. The nonlinear characteristics of LiB pack are described by the traceless transformation method, which avoids the estimation error caused by Taylor series expansion and high-order term abandonment. Compared with Taylor series expansion, the traceless transformation has at least second-order accuracy, and for Gaussian distribution, the third-order accuracy is achieved. The selection of untracked transformation sampling points is realized based on the correlation sequence of the prior mean value and the prior covariance matrix square root, with the principle shown in Figure 3.

The unscented transformation shows good performance in SOC estimation. The sigma data points after transformation are obtained by nonlinear function transformation, and mean and covariance after transformation are obtained by weighted data points, and then their weighted factors are obtained.

**Iterative process.** Combined with the S-OCM of LiB pack, the iterative calculation of SOC is realized based on the UKF. By taking SOC as the variable in the equation of state and the open-circuit voltage as the variable of the observation equation, the expressions of the equation of state and the observation equation are constructed.

The  $x_k$  is the state variable, and  $y_k$  is the observed variable of working voltage output. The system noise parameter  $w_k$  and the observed noise parameter  $v_k$  are both Gaussian white noise, and the covariances are  $Q$  and  $R$ , respectively. By iterative calculation, the estimated  $x_k$  of the Kalman filter model is calculated from the previous state value  $x_{k-1}$ , input signal  $I_k$  and measurement signal  $y_k$ . The UKF algorithm does not need to linearize the nonlinear equation of state function  $f(\cdot)$  and the observation equation function  $h(\cdot)$  and used nonlinear transformation processing to find the detected data points. Then, the Gaussian probability density data sequence of these SOC sample data points is calculated. The selection of sample data points is based on the nonlinear transformation processing and used in the state space description of SOC estimation of LiB pack. The  $2n + 1$  dimension Sigma data set and its weighting coefficients are obtained by nonlinear transformation processing. Based on the above analysis, the Sigma data set is obtained by equation (10)

$$\begin{cases} x^{(i)} = \bar{x} & i = 0 \\ x^{(i)} = \bar{x} + (\sqrt{(n+\lambda)P_x})_i & i = 0, \dots, n \\ x^{(i)} = \bar{x} - (\sqrt{(n+\lambda)P_x})_{i-n} & i = n+1, \dots, 2n \end{cases} \quad (10)$$

wherein  $n$  is the dimension of the state variable.

The above Sigma data set is analyzed and its corresponding weight is obtained by equation (11)

$$\begin{cases} \omega_m^{(0)} = \frac{\lambda}{n+\lambda}, \lambda = \alpha^2(n+k) - n \\ \omega_c^{(0)} = \frac{\lambda}{n+\lambda} + (1 - \alpha^2 + \beta) \\ \omega_m^{(i)} = \omega_c^{(i)} = \frac{1}{2(n+\lambda)}, i = 1, \dots, 2n \end{cases} \quad (11)$$

wherein  $\omega_m$  and  $\omega_c$  are the weights needed to calculate the mean and variance of the Sigma points, respectively.  $\alpha$  is the scale factor.  $k$  is a free parameter.  $\beta$  is a nonnegative weight.  $\lambda$  is the scaling factor.

Since the computational complexity of SOC is positively correlated with the number of data points, it is more beneficial for integrated applications to use fewer data sets in transformation process. Therefore, in this paper, SOC is selected as the only state variable to implement the unscented transformation, which is used for the parameter preprocessing of SOC estimation of LiBs. The estimation process of SOC is as follows.

S1: Construction of Sigma point set, as shown in equation (12)

$$x_{k-1}^{(i)} = \begin{bmatrix} x_{k-1} \\ x_{k-1} + \sqrt{(n+\lambda)P_{k-1}} \\ x_{k-1} - \sqrt{(n+\lambda)P_{k-1}} \end{bmatrix} \quad (12)$$

S2: Bringing the Sigma point set into the equation of state. One-step prediction of the state variable is obtained

$$x_{k|k-1}^{(i)} = f[x_{k-1}^{(i)}, u_{k-1}] + w_{k-1}i = 1, \dots, 2n+1 \quad (13)$$

S3: The state variables are updated in time based on the results of the one-step prediction and the mean and weight of the Sigma point set

$$x_{k|k-1} = \sum_{i=0}^{2n} \omega^{(i)} x_{k|k-1}^{(i)} \quad (14)$$

S4: According to the variance weight of the Sigma point set, the predicted value of the variance of the SOC state is updated

$$P_{k|k-1} = \sum_{i=0}^{2n} \omega^{(i)} [x_{k|k-1} - x_{k|k-1}^{(i)}] [x_{k|k-1} - x_{k|k-1}^{(i)}]^T + Q_{k-1} \quad (15)$$

S5: The UT transform is used again for the state value predicted in one step to obtain a new sequence of Sigma data points for SOC estimation

$$x_{k|k-1}^{(i)} = \begin{bmatrix} x_{k|k-1} \\ x_{k|k-1} + \sqrt{(n+\lambda)P_{k|k-1}} \\ x_{k|k-1} - \sqrt{(n+\lambda)P_{k|k-1}} \end{bmatrix} \quad (16)$$

S6: The Sigma point set after the double unscented transformation is brought into the observation equation of the estimation model for updating the observation variables. The update process is shown in equation (17)

$$y_{k|k-1}^{(i)} = h[x_{k-1}^{(i)}, u_k] + v_{k-1} \quad i = 1, \dots, 2n+1 \quad (17)$$

S7: Calculate the predicted value of  $U_L$  and covariance matrix update.

(1) Observed value update

$$\bar{y}_{k|k-1} = \sum_{i=0}^{2n} \omega^{(i)} y_{k|k-1}^{(i)} \quad (18)$$

(2) Autocorrelation matrix update

$$P_{yy,k} = \sum_{i=0}^{2n} \omega_c^{(i)} \begin{bmatrix} y_{k|k-1}^{(i)} - \bar{y}_{k|k-1} \\ y_{k|k-1}^{(i)} - \bar{y}_{k|k-1} \end{bmatrix}^T + R \quad (19)$$

(3) Cross-correlation matrix update

$$P_{xy,k} = \sum_{i=0}^{2n} \omega_c^{(i)} \begin{bmatrix} x_{k|k-1}^{(i)} - \bar{x}_{k|k-1} \\ y_{k|k-1}^{(i)} - \bar{y}_{k|k-1} \end{bmatrix}^T \quad (20)$$

S8: Calculate Kalman gain matrix

$$K_k = P_{xy,k} P_{yy,k}^{-1} \quad (21)$$

S9: The state variable and error covariance update.

(1) The status variable update process

$$\bar{x}_k = \bar{x}_{k|k-1} + K_k [y_k - \bar{y}_{k|k-1}] \quad (22)$$

(2) Error covariance update

$$P_k = P_{k|k-1} - K_k P_{yy,k} K_k^T \quad (23)$$

### Error correction strategy

Although UKF is more robust than EKF, when using UKF to estimate the charge of LiBs, if the pulse current change rate is large, the tracking effect of the algorithm is not ideal, and the estimation error is large. The

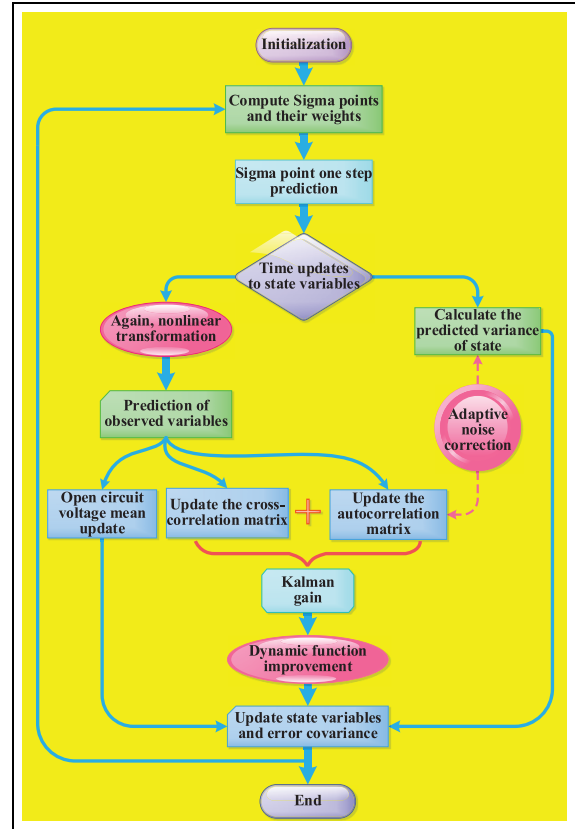


**Figure 4.** The iterative flow of the improved algorithm. The background in the figure does not need to be highlighted.

UKF algorithm is improved to solve these problems, improve the Kalman gain with dynamic function module to improve system stability. The closed-circuit voltage of the system is predicted by two nonlinear transformations to improve the accuracy of the system. Meanwhile, an adaptive algorithm is proposed to predict and correct system noise and observation noise, which makes the system more stable. The detailed flowchart of the improved algorithm is shown in Figure 4.

**Double nonlinear transformation.** In the prediction process of SOC estimation, by using unscented transformation to solve the problem of SOC estimation of mean and variance of nonlinear transformation, don't need to calculate the Jacobian matrix, and there are no higher-order term negligence problems, so that the system has high accuracy and strong stability. Three Sigma data point sequences of SOC values and their corresponding weights  $\omega_c$  and  $\omega_m$  are obtained through a nonlinear transformation. Then, the predicted values of the three Sigma data points are obtained by the state equation, and the single SOC predicted values are obtained by the weighted summation processing. The unscented transformation is performed again on the predicted result, and the transformation results are applied to the observation equation, so as to improve the estimation accuracy. Finally, the closed-circuit voltage predictive value is calculated by weighting and used in the status

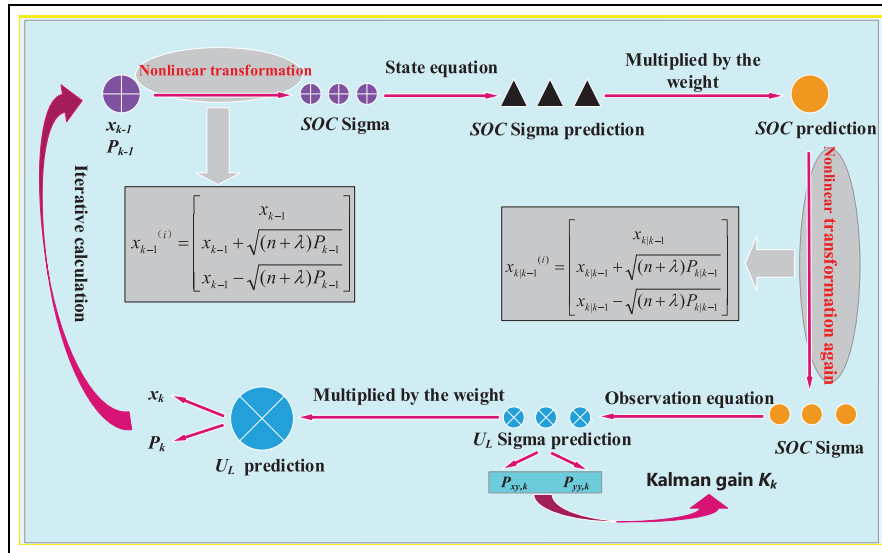


Figure 5. Double nonlinear transformation iterative calculation process schematic.

update of SOC estimation process. The calculation of the second nonlinear transformation is shown in equation (16). The whole process of iterative calculation of double nonlinear transformation is shown in Figure 5.

**Dynamic function correction.** According to the estimation results under simulated dynamic conditions, when the pulse current change rate is high, the estimation error is large. When Kalman filter performs filtering estimation, if the state of the system is suddenly changed, it is often slow to track the real state, thus reducing the estimation accuracy. In this paper, we will improve it to make the algorithm have better tracking effect on the estimation process.

If the change of working current meets the conditions shown in equation (24) below

$$\frac{I_k - I_{k-1}}{\Delta t} \geq \Delta I_{\max} \tag{24}$$

wherein the  $\Delta I_{\max}$  is the maximum current change setting value. Namely, if the working condition current causes jump mutation, then the improved Kalman gain and state estimation measurement are updated as shown in equation (25)

$$\begin{cases} K'_k = \gamma K_k = \gamma(P_{xy,k} P_{xy,k}^{-1}) \\ x_k = x_{k|k-1} + K'_k(y_k - y_{k|k-1}) \end{cases} \tag{25}$$

wherein the  $\gamma$  is the gain factor and its value can be more than 1, so that the convergence speed of the estimated value in the process of algorithm estimation is accelerated. The value should not be too large, otherwise the error will also increase. This article values between 1 and 2.

To enhance the stability of the system, the gain is set as a dynamic value and automatically adjusted according to the change of current. When the current changes a lot in the working condition, the gain can be adjusted

to a large value dynamically, so that the algorithm can estimate the speed of convergence to increase. When the current changes a little more gently, the gain value will gradually return to the original value. Then, dynamic gain calculation and state estimation measurement are updated as shown in equation (26)

$$\begin{cases} K''_k = K'_k \varphi = \gamma K(k)(1 + \alpha^{t_k - t_0}) \\ x_k = x_{k|k-1} + K''_k(y_k - y_{k|k-1}) \end{cases} \tag{26}$$

wherein  $\alpha$  is the number between 0 and 1,  $t_0$  is the time point at the beginning of the mutation and  $t_k$  is the time point after the mutation.  $\varphi = 1 + \alpha^{t_k - t_0}$  is a dynamic function,  $t_k - t_0$  starts out at approximately 0,  $\alpha^{t_k - t_0}$  starts out at 1,  $y$  is close to 2 and then it converges the fastest. With the constant change in  $t_k$ , the larger the value of  $t_k - t_0$ , the closer the value of  $\alpha^{t_k - t_0}$  is to 0, and then, the closer the value of  $y$  is to 1, the gain coefficient returns to the original value, and the convergence speed decreases to the state before the mutation. When the next mutation comes,  $t_0$  time is recorded again and  $t_k$  starts to increase from the time point of new  $t_0$ . By means of exponential function, the gain at the initial time of mutation is larger to accelerate the convergence speed, and then, the gain is smaller to decrease the convergence speed, so that the dynamic gain correction can be realized.

**Adaptive noise prediction.** The covariance  $Q_k$  and  $R_k$  in the estimation of the algorithm have certain influence on the accuracy and stability of the system. When the  $R_k$  value is large, the gain value decreases and the filtering convergence speed is slow, at which time the filtering correction effect is small. When the  $R_k$  value is small, the gain value is large, the filtering convergence speed is fast and the filtering correction effect is large. However, the actual statistical characteristics of noise are unknown, and the set value is usually used in

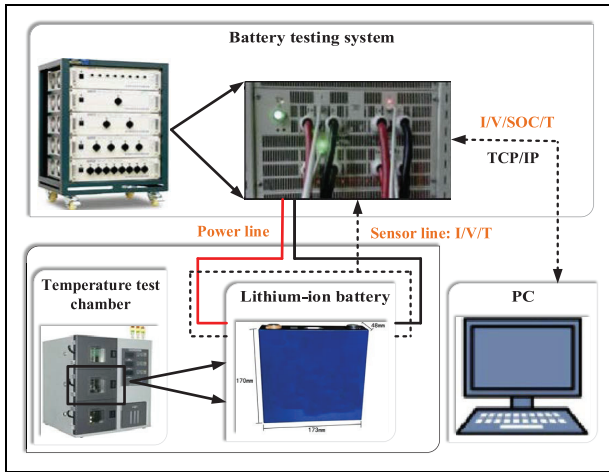


Figure 6. Battery test platform.

estimation. Inaccurate noise variance will reduce the robustness of the system. In this paper, the adaptive algorithm is applied to predict and modify the system noise and observed noise, which enhances the robustness of the system. The estimation principle is as follows:

The system noise and the covariance of the system noise are shown in equation (27)

$$\begin{cases} w_k = (1 - \varepsilon_k)w_{k-1} + \varepsilon_k(x_{k|k-1} - \mathbf{A}_{k-1}x_{k|k-1}) \\ \mathbf{Q}_k = (1 - \varepsilon_k)\mathbf{Q}_{k-1} + \varepsilon_k(K''_{k-1}e_k e_k^T + P_{x_{k|k-1}} - \mathbf{A}_{k-1}P_{x_{k|k-1}}\mathbf{A}_{k-1}^T) \end{cases} \quad (27)$$

The observed noise and the covariance of the observed noise are shown in equation (28)

$$\begin{cases} v_k = (1 - \varepsilon_k)v_{k-1} + \varepsilon_k(y_k - y_{k|k-1}) \\ \mathbf{R}_k = (1 - \varepsilon_k)\mathbf{R}_{k-1} + \varepsilon_k(e_k e_k^T - \mathbf{C}_k P_{x_{k|k-1}} \mathbf{C}_k^T) \end{cases} \quad (28)$$

wherein the calculation of  $e_k$  and  $\varepsilon_k$  is shown in equation (29)

$$\begin{cases} e_k = y_k - y_{k|k-1} - v_{k-1} \\ \varepsilon_k = \frac{(1-\eta)}{(1-\eta_{k-1})} \end{cases} \quad (29)$$

wherein the value of  $\eta$ , which is the forgetting factor, should be between 0.95 and 0.99.

According to  $\mathbf{A}_{k-1}$  in equation (26), the  $\mathbf{C}_{k-1}$  in equation (27) can be calculated, as shown in equation (30)

$$\mathbf{C}_{k-1} = \left[ \frac{\partial f(x_k)}{x_k} \right] \quad (30)$$

The analysis shows that the prediction of system noise and observed noise depends on  $e$ . Although the error of the battery model cannot be eliminated, the experimental verification shows that the adaptive algorithm can estimate the noise, improve the filtering stability and real-time adjustment ability and reduce the SOC estimation error.

## Experimental analysis

### Experimental platform

The UAV ternary polymer LiB is selected for the test; the actual battery capacity after measurement is 68 A h. Using the battery internal resistance tester, the internal resistance of the battery is found to be 0.67 mV. The experimental device structure is shown in Figure 6, which consists of (1) power cell high-power charge and discharge tester (CT-4016-5V100A-NTFA); (2) three-layer independent temperature control test chamber; (3) supporting experimental equipment (BTT-331C); and (4) host computer that displays measurement data and controls charging and discharging processes.

### Modeling verification

The parameters of the main charge HPPC test and the main discharge HPPC test are brought into the S-OCM. The terminal voltage comparison curve obtained from the experiment is shown in Figure 7.

According to the voltage error curve shown in Figure 7(e) and (f), the S-OCM can well estimate terminal voltage during charging and discharging. Among them, the maximum parameter identification error of the HPPC test of the main charging process is less than 0.015 V (nominal voltage is 4.2 V), and the maximum parameter identification error of the HPPC test of the main discharge process is less than 0.01 V, laying the foundation for follow-up research.

### Complex discharge ratio experiments

For the purpose of verifying accuracy and stability of the improved algorithm, complex discharge ratio experiments are designed to more accurately analyze and describe the operating characteristics of UAV LiBs. In the experimental process, SOC estimation performance test under complex converter conditions is realized by combining converter simulation experiments with different discharge current multiples. The experimental correlation curve is shown in Figure 8.

As can be seen from the complex discharge ratio experiment index curves, it can be seen that due to periodic polarization effect of initial discharge point and final discharge point, the estimation error of UKF algorithm is up to 1.8%. The improved UKF algorithm also has the maximum error in the initial estimation, but the SOC estimation error is only 1%. Compared with the traditional algorithm, the improved algorithm can reduce the estimation error by about 0.8%.

### Phased working condition experiments

In order to verify the improved UKF for the reliability of UAV in the process of practical work, the phased working condition experiments are designed. In practical applications, LiBs are used not only for unlocking and starting UAV in normal flight but also for online

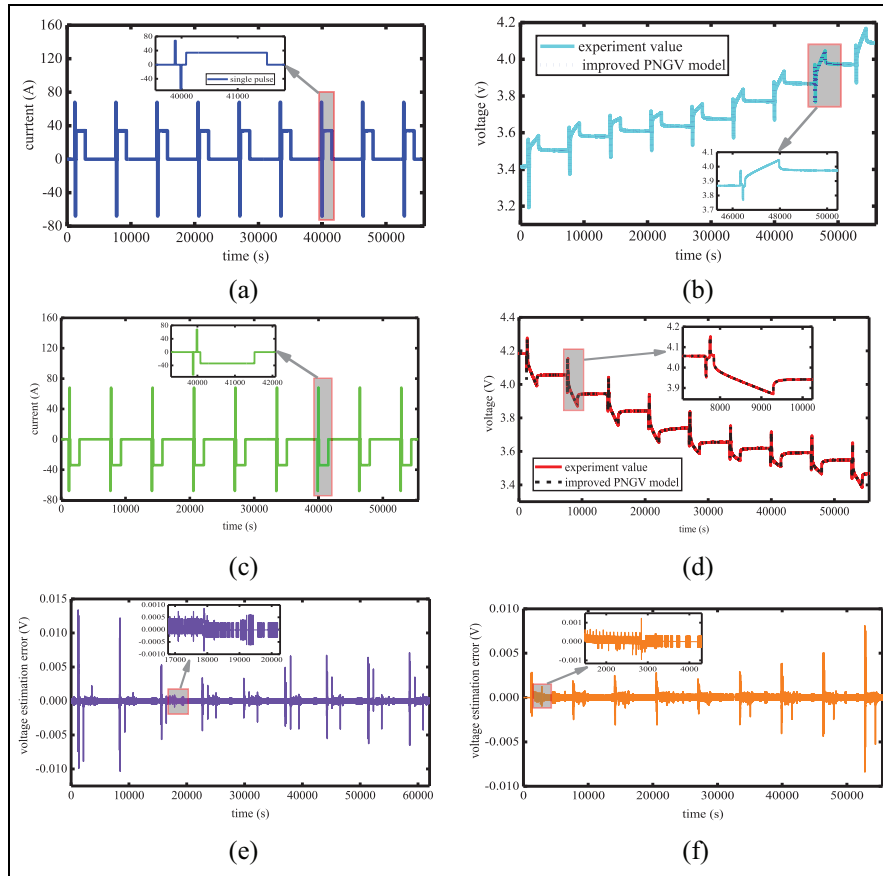


**Figure 7.** The HPPC test index curves of main discharging and charging processes: (a) HPPC test current curve of the main charge, (b) terminal voltage and voltage estimation, (c) HPPC test current curve of the main discharge, (d) terminal voltage and voltage estimation, (e) voltage estimation error of the main charge and (f) voltage estimation error of the main discharge.

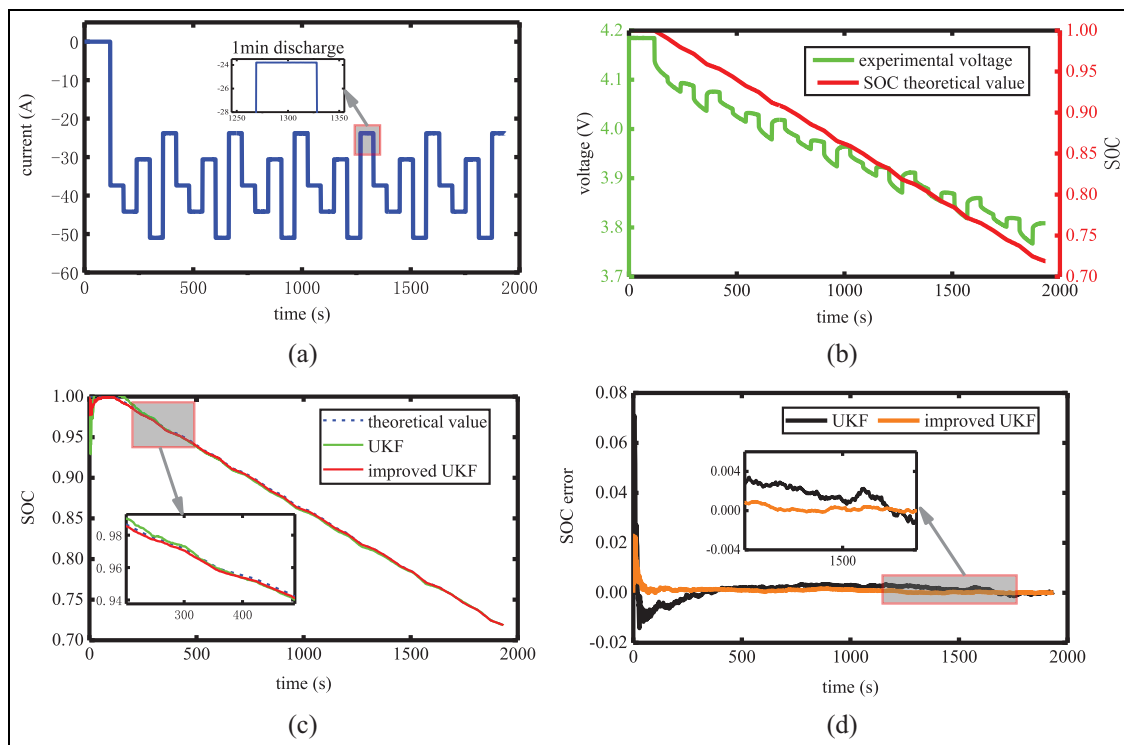


**Figure 8.** The complex discharge ratio experiment index curves: (a) current profile of the complex discharge ratio experiments, (b) the terminal voltage and SOC profiles of the complex discharge ratio experiments, (c) estimated result comparison of different methods and (d) estimated error comparison of different methods.

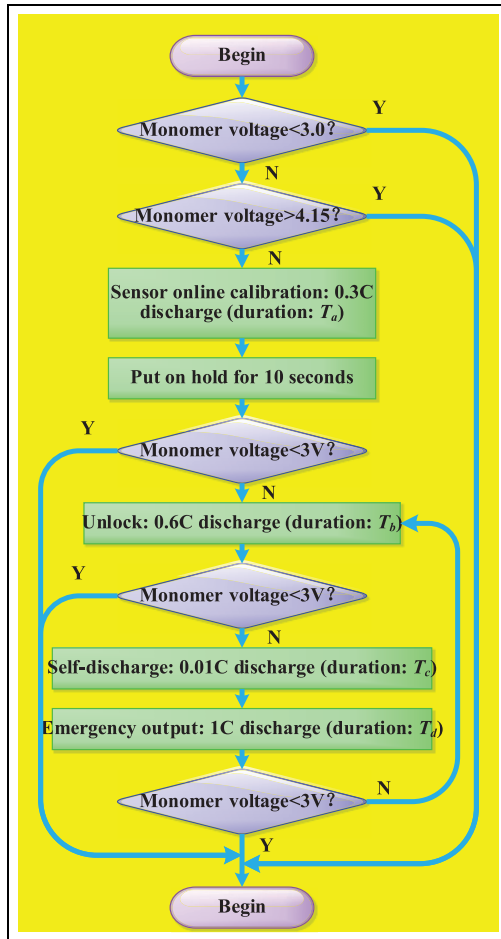


**Figure 9.** UAV experiment tests the flow of working conditions. The background in the figure does not need to be highlighted.

calibration of sensors and emergency output. The overall experimental test process is shown in Figure 9.

In Figure 9,  $T_a$  is the time required for sensor calibration,  $T_b$  is the unlocking start time of UAV,  $T_c$  is the self-discharge time during UAV flight and  $T_d$  is the emergency output time of UAV LiBs. The test process is described below. S1: the system detects whether the total voltage of the UAV LiB is greater than the minimum voltage of 3.00 V. S2: discharge  $T_a$  second at 0.30C to simulate online calibration of UAV sensor. S3: after setting aside for 10.00 s, judge whether the total voltage of LiBs is greater than the minimum voltage of 3.00 V, meeting the conditions and entering step 4. S4: simulate the unlocking and starting of UAV with 0.60-C discharge  $T_b$  second and judge whether the total battery voltage is greater than the minimum voltage at the same time. If the conditions are met, the flight mission enters step 5 or it ends. S5: simulate self-discharge of LiBs at 0.01-C discharge  $T_c$  second, and then enter step 6. S6: use 1.00-C discharge  $T_d$  second to simulate emergency output and judge whether the single voltage and total voltage are greater than the minimum voltage at the same time. If the conditions are met, the flight mission can continue, otherwise it will end. S7: over.

**Table 5.** Working condition set.

Parameter	$T_a$	$T_b$	$T_c$	$T_d$
Working condition	600	20	100	600

The parameters of UAV LiBs under different working conditions are set as shown in Table 5.

According to the data in Table 5, staged working condition tests were performed on the UAV LiB. The results are shown in Figure 10.

The results show that the SOC estimation under UKF has obvious oscillation under the condition of drastic changes in operating current, and the improved method can make the lithium-ion BMS of UAV more robust and ensure the safety of UAV flight mission. As can be seen from the figure above, under the UKF algorithm, the maximum error voltage of the terminal voltage of the ion battery is about 0.07 V, and the error percentage is about 1.8%. The maximum error of the short voltage under the improved UKF algorithm is about 0.03 V, and the error percentage is about 0.7%. In comparison, the improved algorithm is superior not only in robustness but also in accuracy, which meets the requirements of UAV BMS.

### Compound noise effect

Based on the above experiments, the adaptability of the improved UKF algorithm to noise is studied. Due to flaws in processor computing conditions, it is inevitable to have the problem of decimal number reservation and high-order item abandonment in the process of iterative calculation, and then, the process noise is generated, which affects the SOC estimation results. In addition, as the parameters such as voltage, current and temperature of the external measurable signal of LiB pack are affected by the sampling accuracy of the sampling module, it is inevitable that sampling error will occur, which will cause observation noise and further affect the SOC estimation results. Therefore, based on the practical application considerations and based on the verification of SOC estimation accuracy, it is necessary to further carry out the influence experiment of compound noise and carry out the experimental verification of the adaptability of the improved algorithm in terms of working conditions, so as to ensure that the method has a high estimation accuracy under various interference factors.

To verify the adaptability of the improved algorithm to compound noise, set the corresponding relationship between the change values of process noise and observation noise as shown in Table 6.

The SOC estimation results are obtained through experimental analysis, as shown in Figure 11.

In Figure 11, SOC\_0 is obtained by Ampere-Hour integral method. From the results of the experiment, in the case of poor equilibrium state, the modified

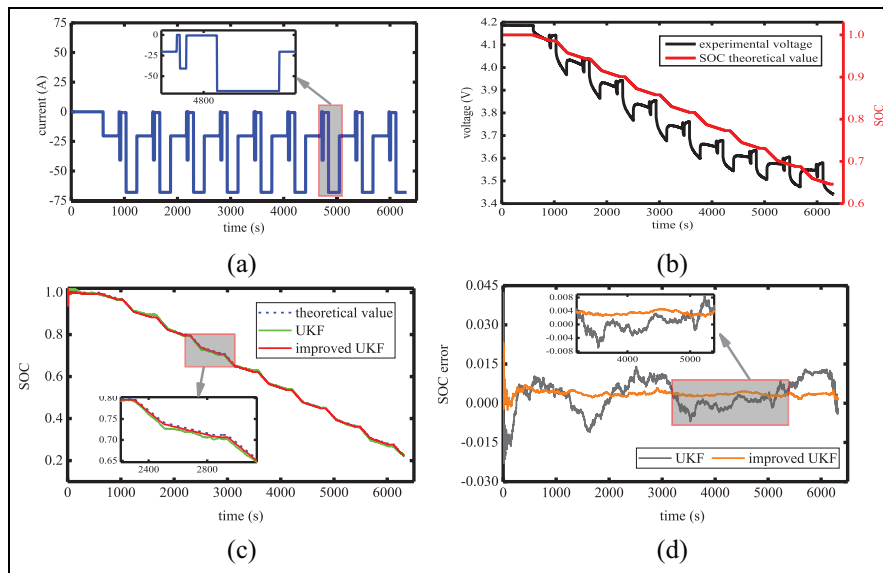


**Figure 10.** The phased working condition experiment index curves: (a) current profile of the phased working condition experiments, (b) the terminal voltage and SOC profiles of the phased working condition experiments, (c) estimated result comparison of different methods and (d) estimated error comparison of different methods.

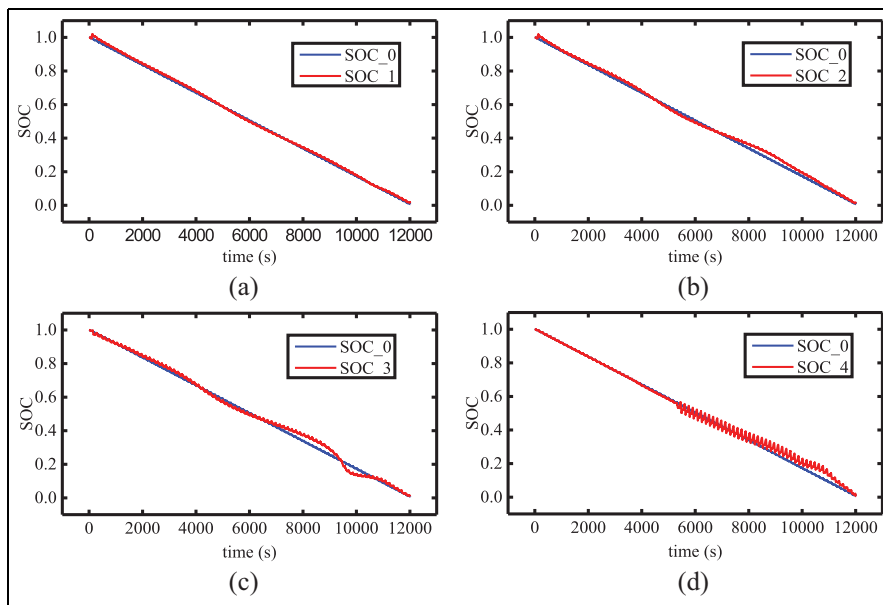


**Figure 11.** Estimated result of different compound noise.

**Table 6.** Correspondence table.

SOC	Q	R
SOC_1	1e-12	0.001
SOC_2	1e-9	0.010
SOC_3	1e-6	0.100
SOC_4	1e-3	1.000

SOC: state of charge.

algorithm has obvious correction effect. When the process noise is small, the experimental value can converge to the actual value in the whole simulation process.

With the increase in process noise, the overshoot of the system starts to increase, but the experimental value converges to the real value quickly under the dynamic modification of the improved algorithm, which further verifies the advantages of the improved algorithm in the estimation effect.

### Conclusion

To fully meet the requirements of parameter measurement in the complex working environment of UAV, an S-OCM is established to describe the battery state in

the dynamic environment. In addition, to solve the problem that the tracking effect of the algorithm is not ideal and the estimation error is large when the pulse current change rate is large, the dynamic function module is used to improve the Kalman gain, and two non-linear transformations are used to predict the closed-loop voltage of the system. To solve the influence of noise on system stability, an adaptive algorithm is proposed to predict and correct system noise and observation noise, which can effectively reduce noise error and enhance system stability. At the same time, the improved UKF method is used to carry out relevant experiments on the adaptability. The equivalent modeling, different CC discharge, UAV working condition and composite noise tests were carried out to verify the feasibility of the model and algorithm in different states. The results show that the algorithm has high estimation accuracy under various simulated working conditions and interference factors. When the current input changes drastically, the estimated error of the improved algorithm can still be maintained at about 1.00%. Compared with UKF, the error is reduced by 0.80%, which is used as the basis for subsequent drone BMS research.

#### Declaration of conflicting interests

The author(s) declared no potential conflicts of interest with respect to the research, authorship and/or publication of this article.

#### Funding

The author(s) received no financial support for the research, authorship and/or publication of this article.

#### ORCID iD

Shunli Wang  <https://orcid.org/0000-0003-0485-8082>

#### References

1. Naoui M, Aymen F, Ben Hamed M, et al. Analysis of battery-EV state of charge for a dynamic wireless charging system. *Energy Storage* 2019; 2: e117.
2. Wei ZB, Zhao J, Zou C, et al. Comparative study of methods for integrated model identification and state of charge estimation of lithium-ion battery. *J Power Sources* 2018; 402: 189–197.
3. Lai X. A comparative study of different equivalent circuit models for estimating state-of-charge of lithium-ion batteries. *Electrochim Acta* 2018; 259: 566–577.
4. Liu XY, Li W and Zhou A. PNGV equivalent circuit model and SOC estimation algorithm for lithium battery pack adopted in AGV vehicle. *IEEE Access* 2017; 6: 23639–23647.
5. Wang YJ, Zhang X, Liu C, et al. Multi-timescale power and energy assessment of lithium-ion battery and super-capacitor hybrid system using extended Kalman filter. *J Power Sources* 2018; 389: 93–105.
6. Zhao LH. Lithium-ion battery state of charge estimation with model parameters adaptation using H-infinity, extended Kalman filter. *Control Eng Pract* 2018; 81: 114–128.
7. Yang RX, Xiong R, He H, et al. A fractional-order model-based battery external short circuit fault diagnosis approach for all-climate electric vehicles application. *J Clean Prod* 2018; 187: 950–959.
8. Wang YJ, Gao G, Li X, et al. A fractional-order model-based state estimation approach for lithium-ion battery and ultra-capacitor hybrid power source system considering load trajectory. *J Power Sources* 2020; 449: 227543.
9. Bahramipanah M, Torregrossa D, Cherkaoui R, et al. Enhanced equivalent electrical circuit model of lithium-based batteries accounting for charge redistribution, state-of-health, and temperature effects. *IEEE T Transp Electr* 2017; 65(1): 589–599.
10. Su J, Lin M, Wang S, et al. An equivalent circuit model analysis for the lithium-ion battery pack in pure electric vehicles. *Meas Control* 2019; 5: 193–201.
11. Meng JH, Stroe DI, Ricco M, et al. A simplified model based state-of-charge estimation approach for lithium-ion battery with dynamic linear model. *IEEE T Ind Electron* 2019; 66: 7717–7727.
12. Wang WH and Mu J. State of charge estimation for lithium-ion battery in electric vehicle based on the Kalman filter considering model error. *IEEE Access* 2017; 7: 29223–29235.
13. Wang YJ, Zhang C and Chen Z. A method for joint estimation of state-of-charge and available energy of LiFePO<sub>4</sub> batteries. *Appl Energ* 2014; 135: 81–87.
14. Zhang SZ, Guo X and Zhang X. Modeling of back-propagation neural network based state-of-charge estimation for lithium-ion batteries with consideration of capacity attenuation. *Adv Electr Comput En* 2019; 19(3): 3–10.
15. Wang SL, Fernandez C, Zou CY, et al. Open circuit voltage and state of charge relationship functional optimization for the working state monitoring of the aerial lithium-ion battery pack. *J Clean Prod* 2018; 198: 1090–1104.
16. Wang SL, Fernandez C, Liu X, et al. The parameter identification method study of the splice equivalent circuit model for the aerial lithium-ion battery pack. *Meas Control* 2018; 510: 125–137.
17. Troy S, Schreiber A, Reppert T, et al. Life cycle assessment and resource analysis of all-solid-state batteries. *Appl Energ* 2016; 169: 757–767.
18. Liu S, Dong X and Zhang Y. A new state of charge estimation method for lithium-ion battery based on the fractional order model. *IEEE Access* 2019; 7: 122949–122954.
19. Wang SL, Tang W, Fernandez C, et al. A novel endurance prediction method of series connected lithium-ion batteries based on the voltage change rate and iterative calculation. *J Clean Prod* 2019; 210: 43–54.
20. Wang SL, Shang L, Li Z, et al. Online dynamic equalization adjustment of high-power lithium-ion battery packs based on the state of balance estimation. *Appl Energ* 2016; 166: 44–58.
21. Tsutsu W, Siegmund T, Parab ND, et al. State-of-charge and deformation-rate dependent mechanical behavior of electrochemical cells. *Exp Mech* 2017; 58: 627–632.
22. Wang YJ, Zhang C and Chen Z. A method for state-of-charge estimation of LiFePO<sub>4</sub> batteries at dynamic currents and temperatures using particle filter. *J Power Sources* 2015; 279: 306–311.

23. Burgos C, Saez D, Orchard ME, et al. Fuzzy modelling for the state-of-charge estimation of lead-acid batteries. *J Power Sources* 2015; 274: 355–366.
24. Ye M, Guo H, Xiong R, et al. A double-scale and adaptive particle filter-based online parameter and state of charge estimation method for lithium-ion batteries. *Energy* 2018; 144: 789–799.
25. Wang YJ and Chen Z. A framework for state-of-charge and remaining discharge time prediction using unscented particle filter. *Appl Energ* 2020; 260: 114324.
26. Meng JH, Luo G and Gao F. Lithium polymer battery state-of-charge estimation based on the adaptive unscented Kalman filter and support vector machine. *IEEE T Power Electr* 2016; 31(3): 2226–2238.
27. Ito A, Kawashima A, Suzuki T, et al. Model predictive charging control of in-vehicle batteries for home energy management based on vehicle state prediction. *IEEE T Contr Syst T* 2018; 26(1): 51–64.
28. Wang SL, Fernandez C, Chen M, et al. A novel safety anticipation estimation method for the aerial lithium-ion battery pack based on the real-time detection and filtering. *J Clean Prod* 2018; 185: 187–197.
29. I-Haur T, Kuan-Hsun Y, Alexander T, et al. Battery cell modeling and online estimation of the state of charge of a lithium-ion battery[J]. *J Chin Inst Eng* 2018: 1–7.
30. Flah A and Mahmoudi C. A novel energy optimization approach for electrical vehicles in a smart city. *Energies* 2019; 12: 929.
31. Wang Q, Luo Y and Han X. Research on estimation model of the battery state of charge in a hybrid electric vehicle based on the classification and regression tree. *Math Comp Model Dyn* 2019; 25(4): 376–396.
32. Flah A and Mahmoudi C. Design and analysis of a novel power management approach, applied on a connected vehicle as V2V, V2B/I and V2N. *Int J Energ Res* 2019; 43: 6869–6889.
33. Yu L and Liu MF. The establishment and analysis of a state of charge model for lithium-ion batteries. *Mod Phys Lett B* 2018; 32: 34–36.
34. Wang TP, Chen S, Ren H, et al. Model-based unscented Kalman filter observer design for lithium-ion battery state of charge estimation. *Int J Energ Res* 2018; 42(4): 1603–1614.
35. Wei ZB, Zou C, Leng F, et al. Online model identification and state-of-charge estimate for lithium-ion battery with a recursive total least squares-based observer. *IEEE T Ind Electron* 2018; 65(2): 1336–1346.
36. Li YW, Huang X, Liu D, et al. Hybrid energy storage system and energy distribution strategy for four-wheel independent-drive electric vehicles. *J Clean Prod* 2019; 220: 756–770.
37. Zhao RX, Kollmeyer PJ, Lorenz RD, et al. A compact methodology via a recurrent neural network for accurate equivalent circuit type modeling of lithium-ion batteries. *IEEE T Ind Appl* 2019; 55(2): 1922–1931.
38. Wang YJ, Liu C, Pan R, et al. Modeling and state-of-charge prediction of lithium-ion battery and ultracapacitor hybrids with a co-estimator. *Energy* 2017; 121: 739–750.
39. Chen C, Xiong R, Yang R, et al. State-of-charge estimation of lithium-ion battery using an improved neural network model and extended Kalman filter. *J Clean Prod* 2019; 234: 1153–1164.
40. Wen JW, Dong G and Chen Z. On-board adaptive model for state of charge estimation of lithium-ion batteries based on Kalman filter with proportional integral-based error adjustment. *J Power Sources* 2017; 365: 308–319.
41. Shen JN, Shen JJ, He YJ, et al. Accurate state of charge estimation with model mismatch for Li-ion batteries: a joint moving horizon estimation approach. *IEEE T Power Electr* 2018; 34(5): 4329–4342.
42. Wei ZB, Meng S, Xiong B, et al. Enhanced online model identification and state of charge estimation for lithium-ion battery with a FBCRLS based observer. *Appl Energ* 2016; 181: 332–341.
43. Zhu Q, Chen JX, Xu ME, et al. Iterative learning based model identification and state of charge estimation of lithium-ion battery. *IET Power Electron* 2019; 12(4): 852–860.
44. Yuan CC, Wang B, Zhang H, et al. State-of-charge estimation of lithium-ion battery based on a novel reduced order electrochemical model. *Int J Electrochem Sci* 2018; 13(1): 1131–1146.
45. Ma ZY, Wang Z, Xiong R, et al. A mechanism identification model based state-of-health diagnosis of lithium-ion batteries for energy storage applications. *J Clean Prod* 2018; 193: 379–390.